中国激光

百纳秒脉宽单频大能量1064 nm激光器

于真真[1]，钟朝阳[1]，王明建[1*]，宋越[1]，刘继桥[1,2]，侯霞[1,2]，陈卫标[1,2**]

[1]中国科学院上海光学精密机械研究所航天激光工程部，上海 201800；
[2]中国科学院大学材料与光电研究中心，北京 100049

摘要 报道了基于光纤-固体混合放大的百纳秒脉冲宽度单频大能量1064 nm激光光源的研究工作。采用1064 nm分布反馈（DFB）半导体激光器作为单频连续种子光光源，采用声光调制器将种子光整形为脉冲宽度约为149.0 ns的洛伦兹波形脉冲光，重复频率为60 Hz，经过级联的全保偏光纤放大器放大后，获得单脉冲能量约为2.1 μJ、脉冲宽度约为216.7 ns的脉冲光输出。固体放大部分采用激光二极管（LD）端面抽运的Nd:YVO_4晶体作为高增益的前放大器进行双程放大，采用LD单侧面抽运的Nd:YAG板条晶体作为预放大器进行双程放大，采用两级LD双侧面抽运的Nd:YAG板条晶体作为功率放大器，最终获得了单脉冲能量为151.4 mJ、脉冲宽度约为267.8 ns的激光输出。采用光学外差法对输出脉冲激光的线宽进行了测试，线宽约为14.2 MHz。研究结果为星载相干测风激光雷达采用1.06 μm的激光光源提供了新的技术路线。

关键词 激光器；百纳秒脉宽；单频；大能量；相干测风

中图分类号 TN248.1 **文献标志码** A **DOI：** 10.3788/CJL231019

1 引言

相干测风激光雷达在航空航天、气象观测、风能开发等领域中具有广阔的应用前景[1-2]。当前，基于星载平台的多普勒测风激光雷达是世界各航天强国竞相发展的高新技术[3-6]，作为激光雷达的核心单元，激光器的性能直接决定着整个雷达系统的测量精度和探测能力。对于相干多普勒测风激光雷达，其利用激光脉冲回波信号与本振光的混频，从频谱上获得风速引起的多普勒频移，频谱越窄，信噪比越高，而激光脉冲宽度与激光频谱成反比。因此为保证测风精度，要求激光的脉冲宽度达到百纳秒以上[7]。此外，星载激光雷达系统对激光光源有着诸多苛刻的要求，如功耗、体积、重量、可靠性等。

基于掺钕晶体的1.06 μm激光光源由于其高成熟度、高效率、小体积、长寿命、高可靠性等优点，在空间中具有广泛应用[8-12]。目前获得单频大能量1.06 μm脉冲激光的方式主要是基于种子注入的Nd:YAG主振荡功率放大（MOPA）系统[12-13]，2012年，Cosentino等[14]报道了为欧空局测风激光雷达（ALADIN）研制的大能量单频紫外激光器，其高能量基频光采用MOPA方案，通过种子注入多程折叠Nd:YAG电光调Q振荡器，获得了1064 nm单频脉冲光，通过两级“之”字形板条激光放大器实现了360 mJ单脉冲能量输出。2018年，Fitzpatrick等[15]报道了基于种子注入Nd:YAG MOPA的空间应用紫外激光器，主振荡器采用种子注入的环形腔Nd:YAG电光调Q获得了1064 nm单频脉冲光，经过传导冷却的三级板条放大器放大后，获得了重复频率为150 Hz、单脉冲能量约为275 mJ的基频光。2022年，Ding等[16]采用非平面环形振荡器（NPRO）作为种子光注入U型腔Nd:YAG主振荡器，得到单脉冲能量为7.0 mJ、脉冲宽度为7.0 ns单频激光输出，经过端面抽运Nd:YAG双程放大以及三级板条放大器后，实现了重复频率为200 Hz、单脉冲能量约为610 mJ、脉冲宽度约为5.8 ns单频脉冲光。上述基于种子注入MOPA系统的振荡级易受环境干扰而失谐，稳定性差，而且整个系统输出的脉冲形状主要由振荡级决定，限制了经过主放大器的脉冲波形的宽度。为了获得更高的能量提取效率，功率放大器普遍工作在增益饱和状态，导致输出脉冲宽度变窄甚至发生形变[17]。在放大系统中，激光脉冲通过放大器后，波形的变化与入射信号脉冲的前沿随时间变化的规律有直接的关系。高斯型脉冲前沿比指数脉冲上升快，经过放大后脉宽可以得到压缩；指数脉冲的形状和宽度变化不大；洛伦兹型脉冲前沿的上升速度比指数脉冲慢，输出波形脉宽加宽[18]。为了得到特定脉冲波形，研究人员提出了基于种子光和放大结构的时域脉冲整形技术[19]，通过对种子脉冲波形进行预调制，实现对输出脉冲波形的控制，相关研究主要集中在激光加工、激光清洗等领域

收稿日期：2023-07-14；**修回日期**：2023-08-16；**录用日期**：2023-09-01；**网络首发日期**：2023-09-15

通信作者：*wmjian@siom.ac.cn；**wbchen@siom.ac.cn

中[20-21]。目前单频大能量百纳秒脉冲宽度的1.06 μm激光激光器还未见报道。

本文针对星载相干测风激光雷达光源的特殊需求，提出了一种百纳秒脉冲宽度单频大能量1.06 μm激光放大系统。采用声光调制器将分布反馈（DFB）半导体激光器输出的连续单频激光进行调制，得到脉冲宽度约为149.0 ns的洛伦兹脉冲波形，通过两级级联光纤放大器进行高增益脉冲放大，实现了2.1 μJ左右的单频脉冲激光输出；采用固体放大器进一步提高脉冲能量，利用自由空间的Nd：YVO$_4$晶体双程前放大器、Nd：YAG板条双程预放大器以及两级板条功率放大器，最终将脉冲能量提升至151.4 mJ，相应的脉冲宽度约为267.8 ns，激光线宽约为14.2 MHz。整个系统采用种子光和光纤/固体混合放大的方案，结构紧凑，稳定性高，脉冲宽度可以根据实际需求进行调节，研究结果为星载相干测风激光雷达光源的研制提供了一种新的技术途径。

2　实验设计与装置

整个系统设计采用全放大链路，其中光纤放大部分的实验装置如图1所示，主要包括单频连续种子源、单模光纤放大以及双包层光纤放大。种子源采用1064 nm分布反馈半导体激光器，其输出功率约为50 mW，线宽约为2 MHz，具有良好的单频特性和可靠性，其输出的单频连续种子光首先进入保偏隔离器（ISO），防止后续放大器的返回光对DFB半导体激光器造成损伤，然后采用全光纤声光调制器1（AOM1）对种子光进行斩波和脉冲整形，AOM的调制频率为200 MHz。AOM1的调制信号由任意波形发生器给出，调制信号为洛伦兹波形，重复频率为60 Hz。调制后的脉冲种子光与半导体激光器1（LD1）的抽运光通过波分复用器1（WDM1）耦合至保偏单模增益光纤（YSF）进行预放大，增益光纤为保偏掺镱离子单模光纤（PM-YSF）。LD为光栅锁定976 nm单模半导体激光器，最大输出功率为660 mW，可在较大范围内保持波长稳定。放大后的脉冲光依次通过保偏隔离滤波器（PMIBP）和AOM2，与LD2的抽运光经WDM2耦合进入保偏双包层增益光纤（YDF）进行光纤主放大，这里PMIBP的作用是滤除放大自发辐射（ASE）并阻挡返回光，AOM2的作用是滤除基底噪声，提高脉冲对比度，其调制信号为方波。此处的增益光纤为掺镱保偏双包层光纤（PLMA-YDF），光纤输出端增加光纤端帽以降低端面的光功率密度，激光经焦距为4.6 mm的准直器准直后输出，进入后续固体放大系统进一步提高激光能量。

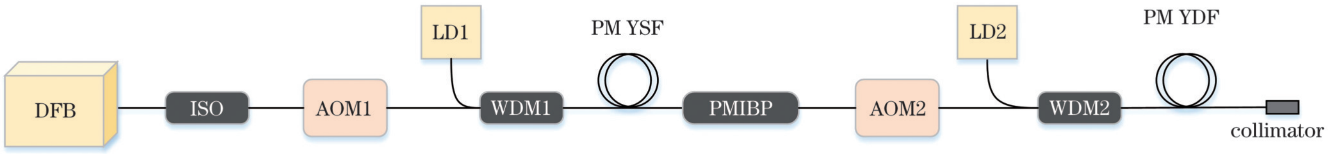

图1　单频脉冲光纤放大实验装置图

Fig. 1　Experimental setup for single frequency pulsed fiber amplification

固体放大系统的实验装置如图2所示，包括Nd：YVO$_4$晶体双程前放大器、Nd：YAG板条双程预放大器以及两级板条功率放大器。具体工作过程如下：

1）光纤准直器的输出依次经过光隔离器1（ISO1）、半波片1（HWP1）、45°1064 nm反射镜（M1）、直角棱镜后入射至Nd：YVO$_4$晶体，直角棱镜的两个直角面均镀有45°高反射（HR）膜@1064 nm。采用直角棱镜的一直角面将激光反射至Nd：YVO$_4$晶体内，晶体出射激光经分光镜（M2）反射后，再次入射至晶体内进行第二次放大，放大后的激光经直角棱镜的另一直角面反射后进入后续放大链路。分光镜M2镀有0°抗反射（AR）膜@808 nm和HR膜@1064 nm。采用Nd：YVO$_4$晶体作为增益介质的目的是实现对小信号的入射激光脉冲的高增益放大。为保证晶体内抽运光的均匀性，Nd：YVO$_4$晶体的掺杂物原子数分数为0.3%，尺寸为3 mm×3 mm×12 mm，晶体两个端面切有5°斜角，并镀有AR膜@1064 nm。晶体四周被铟箔包裹后置于传导冷却的紫铜热沉中。抽运源（LD3）为光纤耦合输出的808 nm半导体激光器，最大输出功率为100 W，尾纤纤芯直径为400 μm，数值孔径为0.22。实验中采用脉冲抽运方式，抽运脉宽为100 μs。抽运光通过焦距比为1：1.5的扩束系统（L1和L2）耦合到晶体内部，聚焦光斑直径约为0.6 mm。

2）Nd：YVO$_4$晶体前放大模块的输出经过级间隔离器2（ISO2）、半波片2（HWP2）后，由偏振分光棱镜（PBS）反射进入Nd：YAG板条预放大器。Nd：YAG板条晶体两端为布儒斯特角切割，激光在晶体内部为“Z”字形传输。为了实现抽运光的高吸收效率，Nd：YAG晶体的掺杂物原子数分数为1.0%，尺寸为3 mm×3 mm×40 mm，两个侧面打毛，其余两个侧面分别为抽运面和冷却面，抽运面镀有AR膜@808 nm&1064 nm，冷却面镀有HR膜@808 nm以实现对抽运光的双程吸收，采用导热胶将冷却面固定在紫铜热沉上，进行传导散热。抽运源采用三组808 nm LD阵列，每组阵列包含4个巴条，单巴条的

峰值功率为 150 W，脉冲宽度为 200 μs。单程通过晶体的激光由 Porro 棱镜反射后再次入射晶体进行双程放大。由于 Porro 棱镜的退偏特性，这里选用了 0.57λ 波片（λ 为波长），通过旋转波片的角度，双程放大的激光偏振态由 S 偏振转换为 P 偏振，从而由 PBS 透射输出。

3）PBS 出射激光被光路转折镜（M3 和 M4）反射，经过级间隔离器 3（ISO3）、半波片 3（HWP3）后进入 Nd:YAG 板条主放大器 1，该放大器采用双侧抽运、双侧冷却、单程放大的 Zig-Zag 结构设计。该放大级的 Nd:YAG 板条晶体两端同样为布儒斯特角切割，采用 808 nm LD 阵列在晶体的全反射点进行双侧面抽运，以提高抽运效率。每组 LD 阵列同样为 4 个巴条，共 10 组。Nd:YAG 晶体的掺杂物原子数分数为 1.0%，尺寸为 6.0 mm×6.0 mm×113.4 mm，抽运面镀有 AR 膜@808 nm&1064 nm，晶体上下两个侧面被夹在紫铜热沉中进行传导散热。为了补偿晶体的热透镜效应，采用柱透镜 1（CL1）对放大后的激光进行整形，激光经过光路转折镜（M5）、1.95 倍扩束系统以及反射镜（M6）后进入 Nd:YAG 板条主放大器 2 进行放大。

4）主放大器 2 仍然采用双侧面全反射点抽运、双侧面传导冷却的 Zig-Zag 板条单程放大器设计，Nd:YAG 板条晶体两个端面为 40°切割，尺寸为 6.0 mm×8.0 mm×121.4 mm，其他参数与主放大器 1 的晶体相同。抽运源 808 nm LD 阵列共 14 组，每组包含 6 个巴条。最终放大后的激光经过反射镜（M7）反射、柱透镜 2（CL2）整形后输出。

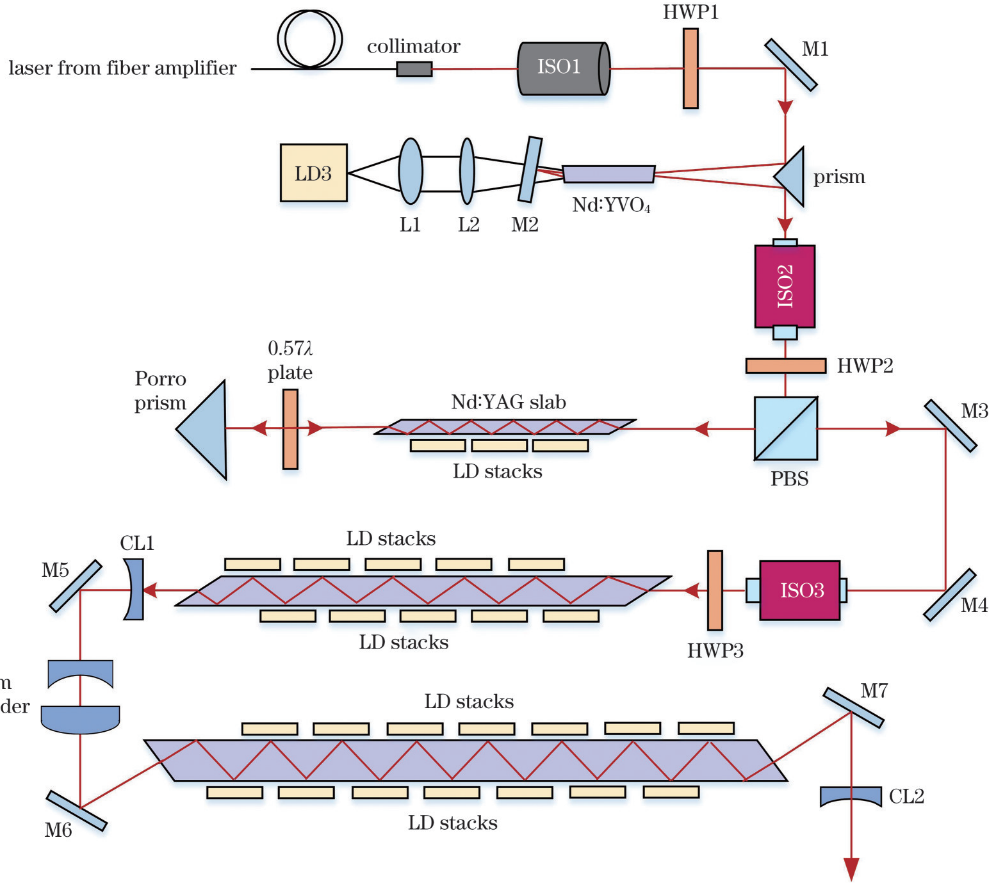

图 2 固体放大实验装置图

Fig. 2 Experimental setup for solid-state amplification

3 实验结果

3.1 光纤放大输出特性

AOM1 和 AOM2 采用的调制信号如图 3 所示。其中：AOM1 的调制信号为洛伦兹波形，其脉冲宽度约为 149.0 ns，其上升沿和下降沿分别为 205.0 ns 和 203.3 ns；AOM2 的调制信号为矩形脉冲，其脉冲宽度约为 2.4 μs。

LD1 与 LD2 采用脉冲抽运方式，当抽运脉冲宽度为 1.2 ms、峰值功率分别为 580 mW 和 525 mW 时，测得放大后的脉冲能量约为 2.1 μJ，脉冲宽度约为 216.7 ns，脉冲的上升沿和下降沿分别为 96.2 ns 和 122.7 ns，如图 4 所示。图 5（a）所示为光纤放大器的输出光经准直器准直后的近场光斑的强度分布情况，光斑直径约为 0.6 mm。采用焦距为 1 m 的透镜测试了远场分布，图 5（b）所示为透镜焦点处的光斑强度分布，计算得到激光发散角约为 2.7 mrad。

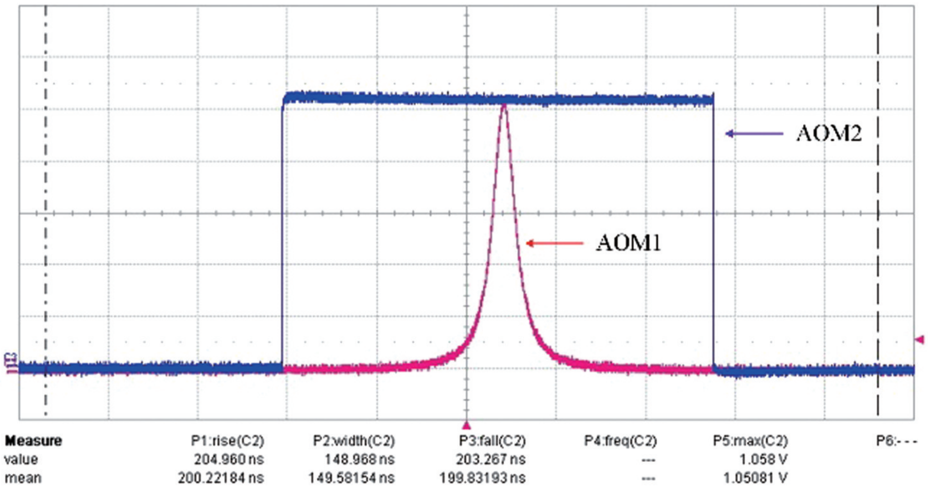

```
Measure     P1:rise(C2)    P2:width(C2)   P3:fall(C2)    P4:freq(C2)   P5:max(C2)   P6:---
value       204.960 ns     148.968 ns     203.267 ns     ---           1.058 V
mean        200.22184 ns   149.58154 ns   199.83193 ns   ---           1.05081 V
```

图 3　AOM1 和 AOM2 的调制信号

Fig. 3　Modulation signals of AOM1 and AOM2

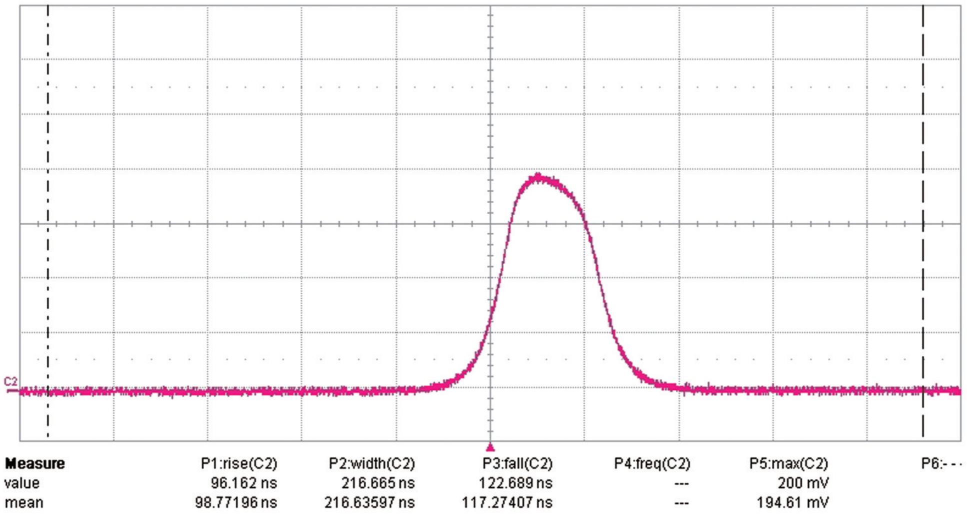

```
Measure     P1:rise(C2)    P2:width(C2)   P3:fall(C2)    P4:freq(C2)   P5:max(C2)   P6:---
value       96.162 ns      216.665 ns     122.689 ns     ---           200 mV
mean        98.77196 ns    216.63597 ns   117.27407 ns   ---           194.61 mV
```

图 4　光纤放大后的激光脉冲

Fig. 4　Laser pulse after optical fiber amplification

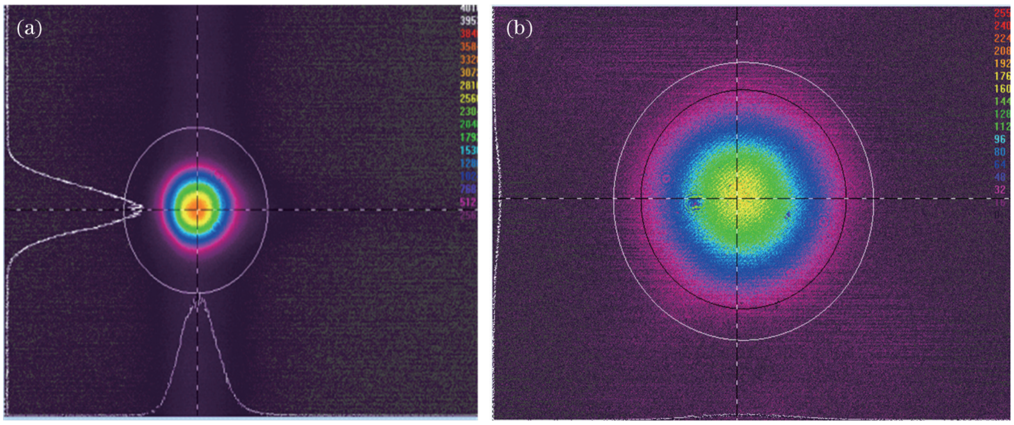

图 5　光纤放大器的输出光经准直器准直后的光强分布。(a)近场；(b)远场

Fig. 5　Intensity distributions of output light of fiber amplifier after collimation by collimator. (a) Near field; (b) far field

3.2　固体放大输出特性

由于光纤放大器输出的能量十分有限，采用晶体增益介质对激光脉冲能量进行进一步放大。实验中当 Nd∶YVO$_4$ 双程放大的抽运能量约为 6.4 mJ 时，放大后的单脉冲能量约为 307.5 μJ，该放大级的提取效率约为 4.8%，测得的脉冲宽度约为 181.6 ns，脉冲的上升沿和下降沿分别为 124.0 ns 和 203.2 ns。当 Nd∶YAG 板条双程预放大器的抽运能量约为 240 mJ 时，放大后的

单脉冲能量约为6.5 mJ，相应的提取效率约为2.6%。当板条主放大器1的抽运能量约为800 mJ时，放大后的单脉冲能量约为57.5 mJ，提取效率约为6.4%。当板条主放大器2的抽运能量约为1040 mJ时，放大输出的单脉冲能量约为151.4 mJ，提取效率约为9.0%。综上，对于固体放大系统，总抽运能量为2086.4 mJ，系统的光光效率约为7.3%。在最大输出能量为151.4 mJ时测得的脉冲宽度约为267.8 ns，上升沿和下降沿分别为191.7 ns和161.4 ns。图6所示为板条主放大器2放大后的脉冲波形。实验结果表明洛伦兹波形的种子光经过放大后脉冲变宽，原因是放大过程中的最大增益呈指数函数形式，洛伦兹波形的脉冲前沿的上升速度比指数脉冲慢，而脉冲前沿放大的速率呈指数变化，因此放大后输出波形的脉宽变宽。

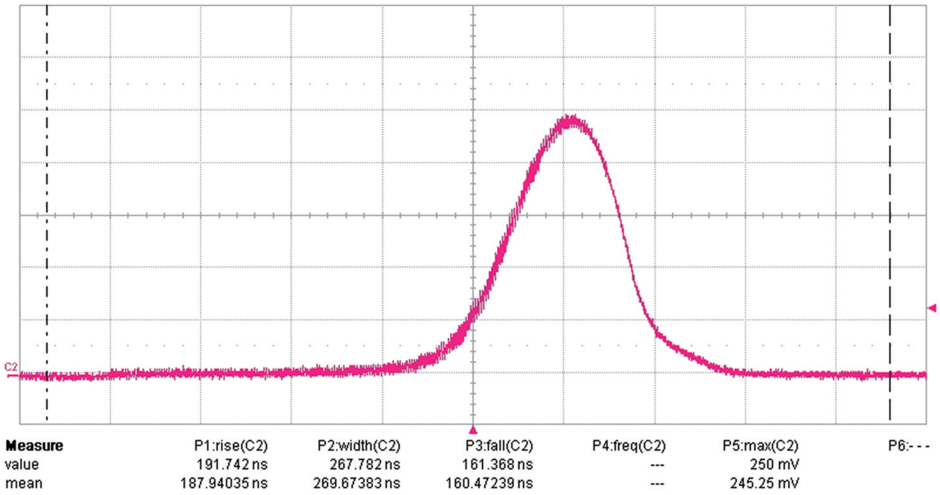

图6　板条主放大器2放大后的脉冲波形

Fig. 6　Pulse profile after amplification by slab main amplifier 2

当板条主放大器2输出的脉冲能量为151.4 mJ时，采用光束质量分析仪对输出激光的光束质量因子进行了测量，水平x方向和竖直y方向上的光束质量因子M_x^2和M_y^2分别为1.39和1.60，如图7所示。图7插图为采用光束分析仪测试的柱透镜整形后的近场光斑，可以看出近场光斑的强度分布均匀，近似呈平顶分布。输出的近场光斑和光束质量表明晶体的热效应对输出光场的分布没有产生严重影响。实验中对固体放大级的抽运能量进行了限制以降低各级晶体的热效应。在主放大器2中，沿晶体散热方向的热透镜焦距约为3 m，对该方向采用柱面镜进行热补偿；“之”字形方向没有观察到热聚焦现象，没有进行相应的热补偿。此外，采用镀有1064 nm增透膜的半波片和偏振片组合对输出激光的偏振特性进行了测量，实验中主放大器1的晶体为布儒斯特角切割，对激光有选偏作用，经过主放大器2放大后激光偏振度在20 dB以上。

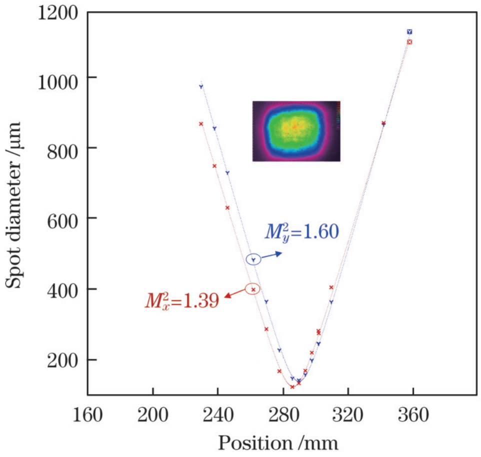

图7　柱透镜整形后板条主放大器2输出激光的光束质量因子（插图为近场光斑）

Fig. 7　Beam quality factors of output laser of slab main amplifier 2 after cylindrical lens shaping (inset is near-field spot)

采用波长计测量了脉冲激光的波长，测量结果如图8所示。可以看出，激光的中心波长为1064.49 nm，该波长计具备线宽测量功能，测得的激光线宽小于500 fm，小于波长计的分辨率。

为测试脉冲激光的线宽，采用实验室自行设计搭建的一套脉冲激光中心频率实时监测系统[22]，该系统基于光学外差测试的方法。参考光同样采用DFB激光器，利用激光器的温度调谐，使其频率和脉冲激光的频率差值为～200 MHz，将它与脉冲激光进行拍频处理，拍频信号由硅光电探测器接收后，被输入到频率监测系统的数据采集卡上，经后续数据处理得到脉冲光的线宽。图9所示为测试得到的约1.7×10^5个脉冲的线宽稳定性，线宽均值约为14.2 MHz，线宽稳定性的均方根（RMS）约为0.25 MHz。

实验中对不同脉宽洛伦兹调制信号下的激光放大进行了研究，通过改变声光调制器1的洛伦兹调制信号的脉冲宽度，研究了经光纤放大和固体放大后脉冲波形的变化，如表1所示。可以看出，放大后的脉冲宽度

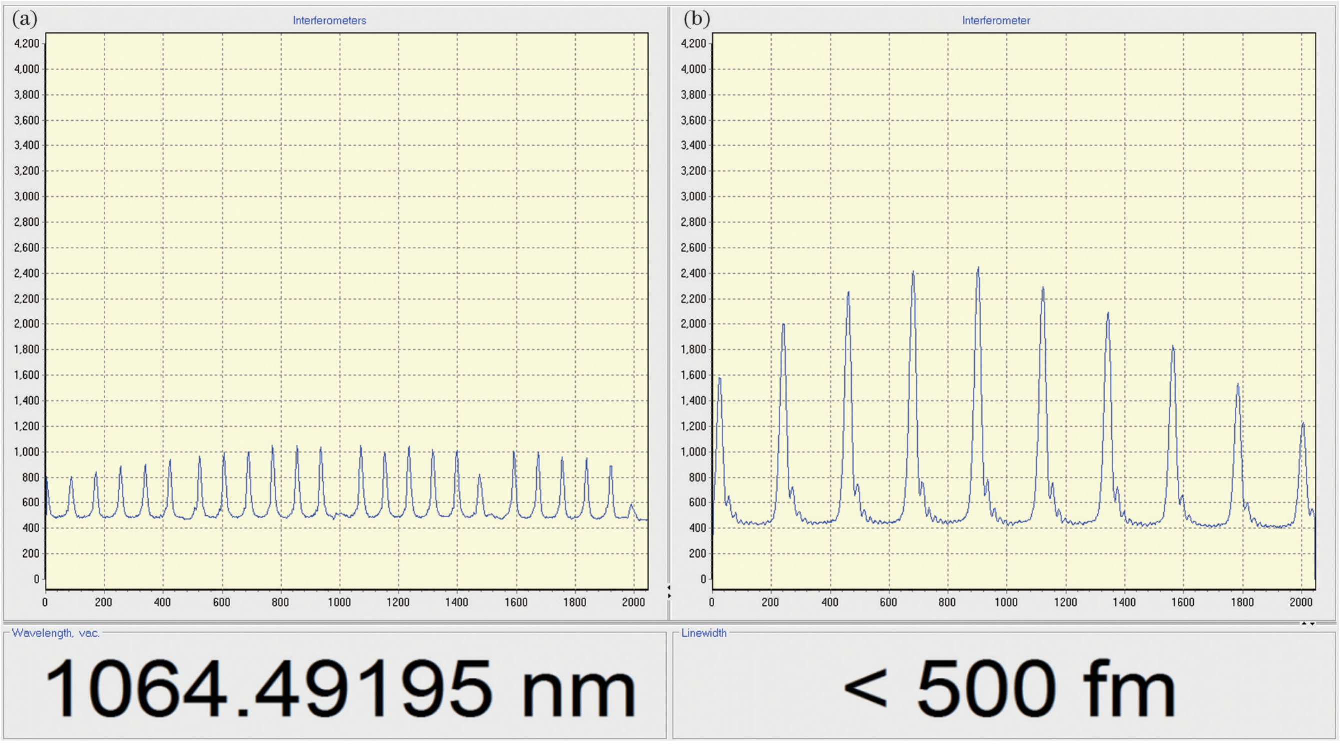

图 8　输出脉冲激光的中心波长及线宽。(a)中心波长;(b)线宽

Fig. 8　Central wavelength and linewidth of output pulse laser. (a) Central wavelength; (b) linewidth

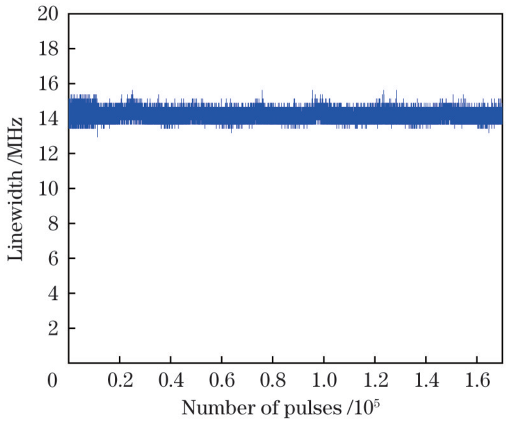

图 9　输出激光的线宽稳定性

Fig. 9　Linewidth stability of output laser

表 1　不同脉宽洛伦兹波形调制下放大后的脉冲参数

Table 1　Pulse parameters after amplification under Lorentz waveform modulation with different pulse widths

Pulse width of Lorentz modulation signal /ns	Pulse after amplification by fiber amplifier			Pulse after amplification by slab main amplifier 2		
	Pulse width /ns	Rising edge /ns	Falling edge /ns	Pulse width /ns	Rising edge /ns	Falling edge /ns
60.5	87.7	42.6	48.6	103.4	76.2	62.4
99.1	144.2	65.8	78.5	163.1	106.8	108.3
149.0	216.7	96.2	122.7	267.8	191.7	161.4
198.2	288.6	130.0	152.2	331.4	202.1	210.3

相对于原始调制信号均有展宽,表明通过改变调制信号的脉冲宽度,可以实现几百纳秒量级脉冲宽度的激光输出,从而满足激光雷达对激光脉冲宽度的特殊需求。

4 结　论

针对星载相干测风激光雷达的光源需求，对基于光纤-固体混合放大的1064 nm百纳秒脉冲宽度单频大能量激光光源进行了实验研究。采用洛伦兹波形调制信号对DFB半导体激光器输出的连续种子光进行整形和斩波处理，得到脉冲宽度约为149.0 ns、重复频率为60 Hz的脉冲种子光，经过级联的光纤放大和多级固体放大后，最终实现了单脉冲能量约为151.4 mJ、脉冲宽度约为267.8 ns的激光输出，采用光学外差法测得激光线宽约为14.2 MHz。通过改变洛伦兹调制信号的宽度，可得到脉冲宽度在百纳秒至几百纳秒量级的激光输出。该光源基于种子光和级联放大的方式，具有结构紧凑和稳定性高的优点，为星载相干测风激光雷达采用1.06 μm的激光光源提供了一种新的技术路线。

参 考 文 献

[1] Liu Z L, Barlow J F, Chan P W, et al. A review of progress and applications of pulsed Doppler wind LiDARs[J]. Remote Sensing, 2019, 11(21): 2522.

[2] 周艳宗, 王冲, 刘燕平, 等. 相干测风激光雷达研究进展和应用[J]. 激光与光电子学进展, 2019, 56(2): 020001.
Zhou Y Z, Wang C, Liu Y P, et al. Research progress and application of coherent wind lidar[J]. Laser & Optoelectronics Progress, 2019, 56(2): 020001.

[3] 刘智深, 陈震, 于翠荣, 等. 多普勒测风激光雷达从车载到星载[J]. 大气与环境光学学报, 2015, 10(2): 126-138.
Liu Z S, Chen Z, Yu C R, et al. Doppler wind lidar: from vehicle-mounted to space-borne[J]. Journal of Atmospheric and Environmental Optics, 2015, 10(2): 126-138.

[4] 陈炳龙, 杨忠东, 闵敏, 等. 星载多普勒测风激光雷达应用需求与研究进展[J]. 激光与光电子学进展, 2020, 57(19): 190003.
Chen B L, Yang Z D, Min M, et al. Application requirements and research progress of spaceborne Doppler wind lidar[J]. Laser & Optoelectronics Progress, 2020, 57(19): 190003.

[5] Morançais D, Mazuray L, Barthès J C. ALADIN, the first wind lidar in space: development status[J]. Proceedings of SPIE, 2006, 10567: 1056703.

[6] 刘东, 陈斯婕, 刘群, 等. 星载环境探测激光雷达及其关键技术[J]. 光学学报, 2022, 42(17): 1701001.
Liu D, Chen S J, Liu Q, et al. Spaceborne environmental detection lidar and its key techniques[J]. Acta Optica Sinica, 2022, 42(17): 1701001.

[7] 张芳沛, 薛海中, 胡永钊, 等. 相干多普勒测风激光雷达[J]. 应用光学, 2009, 30(6): 1045-1050.
Zhang F P, Xue H Z, Hu Y Z, et al. Coherent Doppler wind lidar [J]. Journal of Applied Optics, 2009, 30(6): 1045-1050.

[8] Yu A W, Li S X, Shaw G B, et al. Overview of space qualified solid state lasers development at NASA Goddard Space Flight Center[J]. Proceedings of SPIE, 2009, 7193: 719305.

[9] 程勇, 刘旭, 谭朝勇, 等. 星载激光测高仪固体激光器技术研究与发展[J]. 红外与激光工程, 2020, 49(11): 20201046.
Cheng Y, Liu X, Tan C Y, et al. Research and development of spaceborne solid state laser technology for laser altimeter[J]. Infrared and Laser Engineering, 2020, 49(11): 20201046.

[10] Masson L, Wazen P. High energy high repetition rate diode pumped laser amplifier modules at 1064 nm for space applications [J]. Proceedings of SPIE, 2012, 10564: 105642X.

[11] Lux O, Wernham D, Bravetti P, et al. High-power and frequency-stable ultraviolet laser performance in space for the wind lidar on Aeolus[J]. Optics Letters, 2020, 45(6): 1443-1446.

[12] Hovis F, Burnham R, Storm M, et al. High efficiency laser designs for airborne and space-based lidar remote sensing systems [J]. Proceedings of SPIE, 2011, 8159: 815903.

[13] 龙江雄, 李刚, 杨彬, 等. 种子注入的全固态单频脉冲激光器研究进展[J]. 激光与光电子学进展, 2018, 55(9): 090001.
Long J X, Li G, Yang B, et al. Progress in injection-seeded all-solid-state single-frequency pulse laser[J]. Laser & Optoelectronics Progress, 2018, 55(9): 090001.

[14] Cosentino A, D'Ottavi A, Sapia A, et al. Spaceborne lasers development for ALADIN and ATLID instruments[C]//2012 IEEE International Geoscience and Remote Sensing Symposium, July 22-27, 2012, Munich, Germany. New York: IEEE Press, 2012: 5673-5676.

[15] Fitzpatrick F, Rudd J, Albert M, et al. Lifetime testing of a 355-nm, space-qualifiable laser[J]. Proceedings of SPIE, 2018, 10779: 1077908.

[16] Ding J Y, Yu G L, Zheng R L, et al. A compact, high-power single-frequency laser based on Nd:YAG slab amplifier[J]. Optics Communications, 2020, 464: 125534.

[17] Koechner W. Solid-state laser engineering[M]. 6th rev and updated ed. New York: Springer, 2006.

[18] 蓝信钜. 激光技术[M]. 2版. 北京: 科学出版社, 2005: 182-191.
Lan X J. Laser technology[M]. 2nd ed. Beijing: Science Press, 2005: 182-191.

[19] 张威, 余锦, 郑义. 主振荡功率放大光脉冲时域整形技术[J]. 激光与光电子学进展, 2021, 58(17): 1700004.
Zhang W, Yu J, Zheng Y. Temporal pulse shaping in master oscillator power amplifiers[J]. Laser & Optoelectronics Progress, 2021, 58(17): 1700004.

[20] Meijer R A, Stodolna A S, Eikema K S E, et al. High-energy Nd:YAG laser system with arbitrary sub-nanosecond pulse shaping capability[J]. Optics Letters, 2017, 42(14): 2758-2761.

[21] Nie M M, Liu Q, Ji E C, et al. Active pulse shaping for end-pumped Nd:YVO_4 amplifier with high gain[J]. Optics Letters, 2017, 42(6): 1051-1054.

[22] 陈晓, 谢小兵, 谢伟, 等. 单频纳秒脉冲激光中心频率实时监测技术[J]. 中国激光, 2017, 44(11): 1101003.
Chen X, Xie X B, Xie W, et al. Real-time monitoring technology for center frequency of single-frequency nanosecond pulse laser[J]. Chinese Journal of Lasers, 2017, 44(11): 1101003.

Hundred-Nanosecond Pulse-Width Single-Frequency High-Energy 1064 nm laser

Yu Zhenzhen[1], Zhong Chaoyang[1], Wang Mingjian[1*], Song Yue[1], Liu Jiqiao[1,2],
Hou Xia[1,2], Chen Weibiao[1,2**]

[1]*Space Laser Engineering Department, Shanghai Institute of Optics and Fine Mechanics, Chinese Academy of Sciences, Shanghai* 201800, *China*;
[2]*Center of Materials Science and Optoelectronics Engineering, University of Chinese Academy of Sciences, Beijing* 100049, *China*

Abstract

Objective Space-based Doppler wind light detection and ranging technology is a highly competitive field among the world's leading aerospace powers. As a key component of lidar, the performance of the single-frequency pulsed laser source determines the measurement accuracy and detection capability of the entire system. For coherent Doppler wind lidar, a laser pulse width exceeding 100 ns is required to ensure the accuracy of the wind measurement. Moreover, spaceborne lidar systems place stringent demands on laser sources in terms of reliability, volume, and weight. Due to its advanced maturity, efficiency, and reliability, the neodymium-doped 1.06-μm laser finds extensive applications in space. Thus, this study proposes a single-frequency, high-energy 1.06-μm laser with a pulse width of hundreds of nanoseconds, aiming to offer a technical approach for the space-borne coherent detection lidar laser source.

Methods A fiber-bulk hybrid amplification system is designed, consisting of a cascaded fiber pre-amplifier chain (Fig. 1) and multi-stage solid-state amplifier chain (Fig. 2). For the fiber pre-amplifier chain, a distributed feedback (DFB) semiconductor laser with a linewidth of approximately 2 MHz serves as a single-frequency continuous-wave (CW) seeder. A Lorentzian pulse waveform is adopted as the modulation signal for an acoustic-optical modulator (AOM) to chop and reshape the CW seeder into a Lorentzian pulse sequence at a repetition frequency of 60 Hz and pulse width of approximately 149.0 ns. The obtained pulsed seeder is then coupled to a Yb-doped single-mode fiber (YSF) amplifier to extract energy and is further amplified by a Yb-doped double-clad fiber amplifier (YDF). To enhance the signal-to-noise ratio, another AOM is utilized with a square modulation signal before the YDF amplifier. A fiber end cap is used at the output of the YDF amplifier to reduce the optical power density at the fiber facet, and the output is collimated using a collimator with a focal length of 4.6 mm, which enters the subsequent solid-state amplification system for further pulse energy scaling. The solid-state amplification system is developed using a fiber-coupled laser diode (LD) end-pumped Nd∶YVO_4 crystal, acting as a high-gain double-pass preamplifier, followed by an LD array single-side-pumped Nd∶YAG slab preamplifier with a double-pass configuration. Finally, a two-stage LD array double-side-pumped Nd∶YAG slab serves as the power amplifier. For the Nd∶YVO_4 crystal preamplifier, a double pass is achieved through angular displacement due to the polarization dependency of the vanadate crystal. After the first pass, the amplified beam is returned with approximately a 3° angular change of the beam direction via the dichromic mirror M2, which is coated with 0° anti-reflection (AR) films at 808 nm and high reflectivity (HR) films at 1064 nm. The Nd∶YAG preamplifier has a zigzag pass with Brewster angle faces, and a double pass is achieved by polarization rotation using a Porro prism and 0.57° plate. The two power amplifiers are single-pass and pumped onto the zigzag total internal reflection point. The Nd∶YAG slabs are conductively cooled from top to bottom by making contact with a conductively cooled Cu heat sink. The first slab power amplifier is cut at the Brewster angle, while the second is cut at an angle of 40°, and also has a near-normal incident.

Results and Discussions The modulation signals for AOM1 and AOM2 (Fig. 3) are Lorentzian waveforms with a pulse width of approximately149.0 ns and rectangular waveforms with a pulse width of 2.4 μs, respectively. With pumping at a 1.2 ms pulse width and peak power of 580 mW for LD1 and 525 mW for LD2, the fiber amplifier produces 2.1 μJ pulse energy with a 216.7 ns pulse width (Fig. 4). After collimation, the measured diameter of the near-field spot is approximately 0.6 mm, and the divergence is approximately 2.7 mrad (Fig. 5). To further scale the pulse energy, the output of the fiber amplifier undergoes amplification using a multi-stage solid-state amplification system. The maximum pulse energy of 151.4 mJ is successfully achieved, with an optical-to-optical efficiency of approximately 7.3% relative to the total incident pump energy. The pulse width of the second slab amplifier output is approximately 267.8 ns with a rising edge of 191.7 ns and a falling edge of 161.4 ns (Fig. 6). The measured laser beam quality factor (M^2) is 1.39 and 1.60, respectively, in the x direction and y direction at a pulse energy of 151.5 mJ with a laser beam quality analyzer (Fig. 7). The inset of Fig. 7 displays the near-field intensity distribution of the laser beam. Using a laser wavelength meter, the center wavelength of the pulse laser measures at 1064.49 nm, and the obtained linewidth of less than 500 fm is limited by the laser wavelength meter itself. To achieve an accurate linewidth, a self-built real-time monitoring system for the laser spectrum is employed. Based on optical heterodyne, the center frequency and linewidth of the laser pulse can be calculated according to the beat signal of the laser pulse and reference CW seeder. The linewidth stability of about 1.7×10^5 pulses is determined (Fig. 8), and the mean value of the linewidth is approximately 14.2 MHz with a stability of about 0.25 MHz (root mean square). By adjusting the pulse width of the Lorentz modulation signal of the AOM1 (Table 1), the study on the amplified pulse waveform reveals that the laser output achieves a pulse width in the range of several hundred nanoseconds, thus meeting the specific pulse width requirement of coherent detection lidar.

Conclusions A hundred-nanosecond, single-frequency, high-energy 1064 nm laser based on fiber-bulk hybrid amplification undergoes experimental investigation as a laser source for space-based coherent detection wind lidar. A Lorentzian pulse waveform reshapes and chops the output of the CW DFB laser. A pulsed seeder with a pulse width of approximately 149.0 ns and a repetition rate of 60 Hz emerges. After the amplification of the cascaded fiber amplifier and multi-stage solid-state crystal amplifier, the system produces a laser output with a single pulse energy of about 151.4 mJ and a pulse width of about 267.8 ns. Utilizing the optical heterodyne method, the laser linewidth measures approximately 14.2 MHz. By altering the pulse waveform of the Lorentz modulation signal, the pulse width of the output laser can vary within several hundred nanoseconds. The study results offer a new technical route for employing a 1.06 μm laser source for space-based coherent detection wind lidars.

Key words lasers; hundred-nanosecond pulse width; single frequency; high energy; wind coherent detection